A TECHNIQUE TO MEASURE STRAIN DISTRIBUTIONS IN SINGLE WOOD PULP FIBERS

Laurence Mott
Post-doctoral Research Associate

and

Stephen M. Shaler
Associate Professor

Department of Forest Management
University of Maine
Orono, ME 04469-5755

and

Leslie H. Groom
Research Technologist
USDA Forest Service
Southern Research Station
Pineville, LA 71360

(Received December 1995)

ABSTRACT

Environmental scanning electron microscopy (ESEM) and digital image correlation (DIC) were used to measure microstrain distributions on the surface of wood pulp fibers. A loading stage incorporating a fiber gripping system was designed and built by the authors. Fitted to the tensile substage of an ESEM or a Polymer Laboratories MINIMAT tester, it provided a reliable fiber straining mechanism. Black spruce latewood fibers (*Picea mariana* (Mill) B.S.P.) of a near-zero microfibril angle displayed a characteristically linear load elongation form. ESEM was able to provide real-time, high magnification images of straining fibers, crack growth, and complex single fiber failure mechanisms. Digital images of single fibers were also captured and used for subsequent DIC-based strain analysis. Surface displacement and strain maps revealed nonuniform strain distributions in seemingly defect-free fiber regions. Applied tensile displacements resulted in a strain band phenomenon. Peak strain (concentration) values within the bands ranged from 0.9% to 8.8%. It is hypothesized that this common pattern is due to a combination of factors including the action of microcompressive defects and straining of amorphous cell-wall polymeric components. Strain concentrations also corresponded well to locations of obvious strain risers such as visible cell-wall defects. Results suggest that the ESEM-based DIC system is a useful and accurate method to assess and, for the first time, measure fiber micromechanical properties.

Keywords: Fibers, micromechanics, strain, digital image correlation, tensile testing, environmental scanning electron microscopy.

INTRODUCTION

Single fiber tensile tests conducted under polarized light confirmed that the microfibril angle of the S_2 secondary cell-wall layer largely controls the mechanical properties of individual wood pulp fibers (Page et al. 1977). By the same technique, fiber defects have also been shown to influence fiber properties including maximum strain potential and fiber failure

mechanisms. However, progress with regard to characterizing mechanical properties of recycled fibers (Wuu et al. 1991) and other fiber characteristics, such as fracture criteria, is slow; and no empirical data exist that can quantify such basic relationships as (collapsed) fiber cell-wall Poisson ratios. Evidence of individual defect impact on the mechanical response of the cell wall is lacking, and at present statistical descriptions of fiber defect/length relationships represent the extent of fiber micromechanics understanding (Page and El-Hosseiny 1976). The objective of this study was to develop a single fiber tensile testing technique capable of extracting micromechanical property data from reliable single fiber tensile tests. Of particular interest was the ability to observe fracture sequences in single fibers and measure microstrain distributions surrounding natural and processing-induced defects.

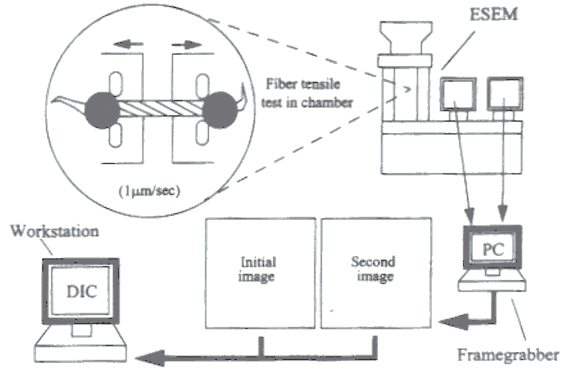

FIG. 1. The experimental set-up for ESEM-based digital image correlation (DIC) evaluation of single fiber microstrains and failure. It consists of a microextensometry located in an ESEM. Single fibers are secured by a free-fiber-alignment ball and socket assembly. Digitally captured images of tensile tests were ported to a workstation for analysis by DIC via a PC-based framegrabber.

MATERIALS AND METHODOLOGY

Single fibers were observed under load using environmental scanning electron microscopy (ESEM). The ESEM is similar to conventional scanning electron microscopes (SEM) in that high magnification and large depth of field images can provide insight into material characteristics. However, the unique design of the ESEM column and secondary electron detector permit the specimen chamber to operate under increased pressures of 5–20 Torr (Cameron and Donald 1994). Water vapor is often used to provide the chamber atmosphere, in which case it is possible to image biological specimens without subjecting them to potentially harmful dehydration processes or conductive coating. A chamber water vapor pressure of approximately 6 Torr was used in this study. Under such conditions single wood pulp fibers were examined in the ESEM in their near natural state. Additional information on this instrument is available in the literature (Cameron and Donald 1994; Sheehan and Scriven 1991).

ESEM observation of single fiber testing

In an effort to establish the reliability of mechanical property data obtained from the developed free-fiber-alignment gripping mechanism, various single fiber types were tested using the loading stage in combination with the ESEM and a Polymer Laboratories MINI-MAT tensile tester. The fiber gripping system was based upon a ball and socket mechanism (Fig. 1). Epoxy droplets applied close to the fiber ends prior to testing provided the ball joints. Although this assembly has been proven to reduce fiber failure at the grips by up to 40% (Mott 1995), it does not completely remove the influence that gripping mechanisms have upon stress and strain distributions within the fiber. For the purposes of this study, however, surface strain was most frequently measured close to the fiber midspan, and a common fiber length to width ratio was approximately 30:1. For such geometries, even in highly anisotropic plates where the average fibril angle approaches 15°, the effect of gripping on strain component distribution at midspan is negligible (Wu and Thomas 1968). The effect is further reduced in near-zero microfibril angle fibers because the collapsed fiber is not a single orthotropic plate. Instead, the opposite walls of the fiber restrict the shear deformation that results from gripping, which

frequently leads to normal stress-strain nonuniformity.

More details on this technique and preliminary findings of this study, which include ESEM failure and crack initiation sequences and a critical assessment of fiber macromechanical property data, are reported elsewhere (Mott 1995; Mott et al. 1995; Groom et al. 1995). This paper describes a micromechanical investigation of fiber cell-wall material using digital image correlation.

Single fibers were introduced into the ESEM specimen chamber under an ambient equilibrium moisture content. A carefully controlled (vacuum) pump-down schedule for the ESEM chamber was used to maintain fibers in their natural hydrated state (Cameron and Donald 1994). The specimen chamber pump-down sequence was characterized by an 8-stage water vapor flooding cycle while simultaneously positioning the fiber out of the beam path to reduce the potential for radiation damage. The final ESEM operating parameters for observing single fibers were a chamber pressure of 5 to 6.3 Torr and a substage temperature of approximately 21°C. Under these carefully monitored environmental conditions, a single fiber equilibrium moisture content of approximately 8.5% was calculated using the Carrier equation (Siau 1984).

The wet bulb depression temperature (a required variable in the Carrier equation) under established ESEM test conditions was determined by first obtaining the corresponding dew point temperature using a Peltier cooling substage. Corresponding dry bulb and the dew point temperatures were then used to find the equivalent wet bulb depression temperature (12°C) with the aid of a psychrometric chart (Siau 1984). A condenser lens strength of 56–60% (instrument setting) and an accelerating voltage of 15 keV were used when examining the fibers.

Digitally captured ESEM images for DIC

For surface-microstrain assessment purposes, single black spruce (*Picea mariana* (Mill) B.S.P.) latewood fibers were obtained by batch kraft pulping the 55th growth ring of a mature tree to a 47% yield (kappa number 56). During preparation, single fibers were also flattened and dried into ribbon shapes prior to tensile testing. More information concerned with fiber drying, moisture content equilibration, and adhesive application is reported in Mott (1995) and Mott et al. (1995). Fiber drying and flattening facilitate easy handling and permit treatment of the fiber as an orthotropic bilaminate material (Page et al. 1977). Flattened fibers also simulated collapsed single fiber geometries in paper sheets and other biocomposites.

Digitally captured (640 × 480 pixel) images of fibers under a uniaxial tensile displacement were used to assess surface microstrains. The experimental setup is presented in Fig. 1. Obtaining suitably high signal to noise ratio images of straining fibers required that a slow electron beam scan rate of 4.3 s/frame be employed. This precluded any further need for image averaging, which is often necessary when employing DIC analysis (James et al. 1989). Following completion of the pump-down and flooding procedure, single fibers were assumed to be under the calculated equilibrium conditions (this process can take up to 2 min). The tensile substage was then moved into the beam path. A low magnification (×300) and an increased scan rate (2.3 frames/s) were selected together with an increased working distance of approximately 10 mm. This procedure was adopted to reduce the potentially damaging effects of the electron beam. Despite visible image noise, fiber surface features such as pitfields were plainly evident, and a fiber gauge length was accurately measured using resident ESEM software (±1 μm).

A suitable area over which strain analysis was to be performed was quickly identified, and the necessary ESEM parameters were adjusted to obtain optimum image quality. A final magnification of approximately 2,500 was usually selected prior to commencing tensile displacement at a rate of 1 μm/s (console controlled). Optimum brightness, contrast levels, beam and condenser strengths were achieved

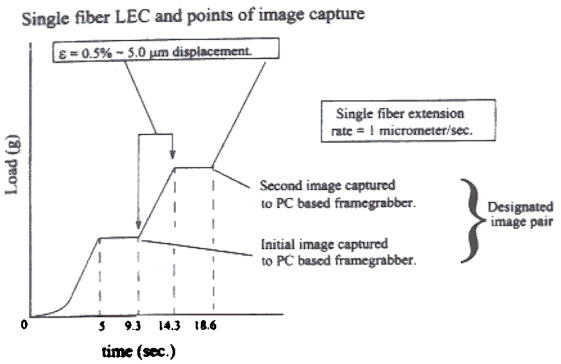

FIG. 2. Characteristic shape of a single fiber load elongation curve. Straining of the fiber is suspended prior to capturing a digital image to obtain distortion-free images. Elapsed time between stopping and resuming straining of the fiber is approximately 4.5 s or 1 frame.

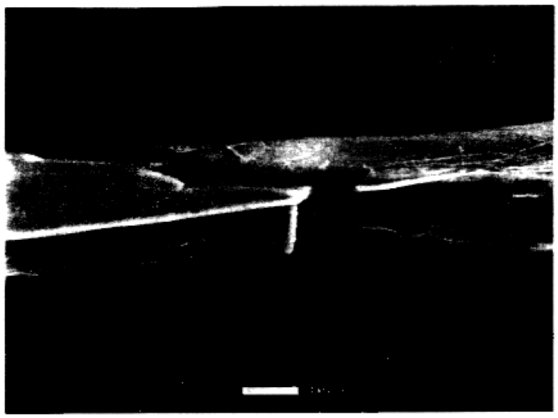

FIG. 3. A single black spruce latewood fiber (low fibril angle) strained to failure. The brash fracture surface is characteristic of fibers with a slow S_2 layer microfibril angle.

manually and then held constant throughout the testing procedure.

Measurement of the microstrain field distributions using DIC required obtaining two successive digital ESEM images over an approximate 5-s displacement (or loading) interval. These images were designated an image pair (Fig. 2). Prior to obtaining any images for DIC, each fiber was loaded so as to achieve a linear load elongation trace. Extension was then suspended and an initial image captured to a remote PC resident framegrabber (approximately 1/30 s capture time). Suspending the tensile test is essential when employing slow scan rates in dynamic microscopy. Failure to do so results in time-delay distorted images where pixels in the lower portion of an image are temporally distorted due to the fact that they are representative of a specimen that has been subject to a proportionally greater strain.

After capturing the initial image, displacement was resumed employing a cross-head extension rate of 1 μm/s for approximately 5 s. Prior to capturing a second image, extension was again suspended. The acquired image pair was then used to perform a DIC analysis of fiber surface displacements resulting from both the 5-μm fiber extension and the small irregular (purely) translational movements of the tensile substage.

Following image acquisition, each fiber was also strained to failure in the ESEM. This required subjecting each fiber to approximately 15–20 s more beam time. Fracture surfaces were then used to assess whether beam damage had significantly affected mechanical properties. The black spruce fibers used in this study demonstrated a brash fracture surface, as is common with mature fibers of low microfibril angle (Fig. 3). The fibers were also prone to cracking and failure at locations other than regions examined by ESEM. These facts provided an initial confirmation that beam-related radiation damage was not significantly affecting the mechanical response of the fiber cell-wall material. Average strain to failure for 218 black spruce latewood fibers as determined by the MINIMAT testing facility was approximately 4.25%.

Principles of DIC

Surface displacements of fibers were determined using a digital image correlation (DIC) technique. Digital image pairs were analyzed using a DIC program written to utilize a Silicon Graphics workstation (Mott 1995). Bi-cubic splines were used to generate continuous surface intensity fields from the discrete digital

images. The intensity field of the first image of a pair was warped using an affine mapping function. The difference in intensity values between the warped first image and the unwarped second image were then calculated, squared, and summed over a defined subregion (Chu et al. 1985). This error was minimized through an iterative process of choosing the six affine warping function coefficients using a Powell algorithm (Press et al. 1990). The warping function coefficients resulting in minimum error (maximum correlation) then define the movement of a central (control) point of the defined subregion. This process is repeated for a range of control points. The resulting whole-field displacement maps are then used to calculate strains using large-strain definitions of strain displacement equations (Fung 1965).

The scale of a random surface body pattern, either artificially applied or natural, dictates the density of chosen displacement measurement (control) points and the required size of extracted subregions. To measure microstrain distributions on a single fiber surface frequently required choosing control points that were substantially less than 1 μm apart (single fibers were approximately 15–30 μm wide when flattened into the familiar ribbon shape). An artificially applied surface pattern would therefore have to consist of extremely small particles. Such a pattern could not be produced at the time of this study. Instead, single fibers were dried in a manner that utilized the effects of anisotropic fiber shrinkage. This created suitable surface patterns in the form of fine surface creases and wrinkles (Koran 1974). The shrinkage creases (Fig. 4) were randomly distributed, produced acceptable ESEM contrast levels to promote accurate correlation, and were of a scale fine enough to permit the use of small image subregions and the close positioning of chosen correlation (control) points.

DIC was performed using extracted image subregions. The optimum size was determined by performing multiple correlations on single image pairs. A range of subregion sizes from (7 × 7) 7^2 to 37^2 pixels were chosen over a range of intensity difference cross-correlation function tolerance values. A total of 36 correlation analyses were performed, each consisting of the same 441 subimage locations. Generated response surface models indicated an image subregion area of approximately 29^2 pixels, provided a near minimum correlation error with reasonable computation time. In addition, the area exhibited a unique surface pattern but was small enough to encompass approximate uniform strains in the x,y plane, an assumption of the DIC technique.

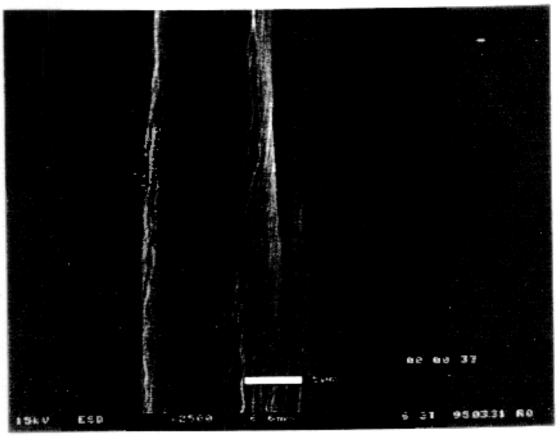

FIG. 4. A digitally captured image of a single wood fiber. The fiber was slowly dried between glass slides to exploit the phenomenon of anisotropic shrinkage. The resulting shrinkage patterns created sufficient image contrast to permit subsequent DIC assessment of surface displacements.

DIC accuracy and calibration

To obtain the necessary sub-pixel accuracy, a continuous intensity function bi-cubic interpolation routine was applied to respective ESEM image pairs. This made it feasible to measure intensity values between discrete pixel locations and to measure respective displacements with a sub-pixel precision of ± 0.1 pixel. At a magnification of 2,500 this was equal to approximately ± 0.008 μm. This value was determined by a rigid body translation technique, conducted digitally and then mechanically inside the ESEM chamber.

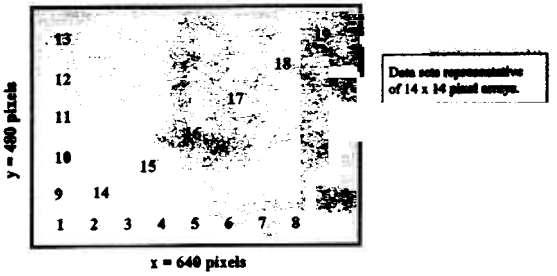

FIG. 5. Approximate position of the 19 (14 × 14 pixel) data sets to determine mean displacement tolerance values.

Digital warping of a single duplicated image was performed by means of a Silicon Graphics library routine. This provided evidence of the DIC program's ability to determine displacements in a rapid and efficient fashion. Applied strains in the x,y plane were recovered with no reported error. This was to be expected in such noise-free images. True noise-influenced (displacement) measurement precision was established using mechanically translated ESEM images. Translation was conducted by moving the tensile substage small amounts in the x,y plane. Mean tolerances in the x and y axes were then determined by running 19 sets of correlation arrays per image pair (4 image pairs). Each set consisted of a regular 14 × 14 pixel array (Fig. 5). Analyses of variances (ANOVA) and subsequent multiple comparison of means tests (Tukey's multiple range test) indicated that no statistically significant differences existed between the reported mean values for u and v displacement between any of the chosen 19 data sets ($P = 0.00$). It was concluded, therefore, that the system was not affected by spatially nonrandom noise. This was confirmed in subsequent tests using the same 19 data set locations applied to translations of varying magnitude. Mean u and v standard deviation were reported as tolerance value of 0.08 pixels and 0.1 pixels, respectively.

To visualize single fiber surface displacement due to microextensometry-induced deformation, the u and v (horizontal and vertical) components of displacement were plotted as 3-D surface maps. Examples of u and v displacement component vectors for a black spruce late-wood fiber are presented in Fig. 6. The u-component of displacement represents passive deformation in the fiber transverse axis resulting from an applied tensile displacement in the fiber longitudinal axis (v). Displacement vector v represents the longitudinal response of the cell wall to same applied tensile displacement.

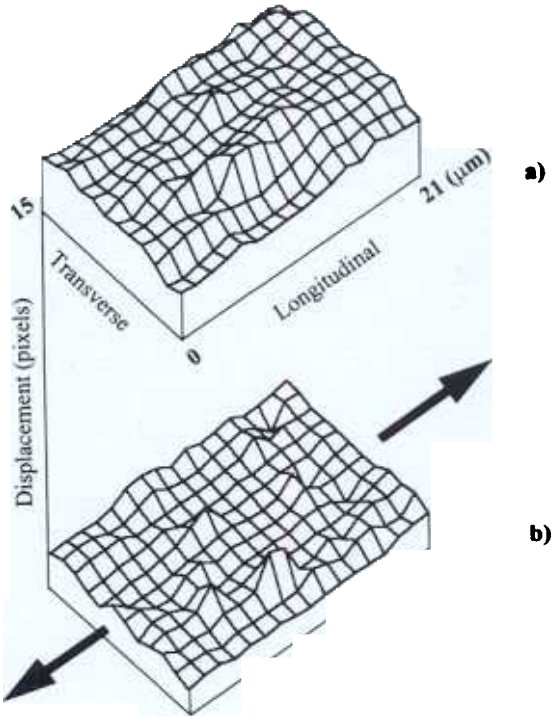

FIG. 6. A 3-D view of the u- and v-microextensometry displacement components. a) shows the u-component vector of (transverse) fiber displacement; b) displays the longitudinal) displacement component coincident to the direction of applied strain (fiber longitudinal axis). Kraft pulped black spruce 47% yield. The arrows represent the direction of applied displacement. Displacement tolerance = 0.1 pixel.

Determination of strains

Surface strain values were determined by first calculating the change in distance (in pixel units) between respective neighboring subre-

gion locations resulting from tensile displacement. The Lagrangian strain tensor definition was then used to obtain normal strains in the x and y directions. The system dependent subpixel precision level (± 0.1 pixel) required that the control points of subregions have a 20 pixel spacing in order to obtain a strain measurement precision of ± 0.5% or better. To obtain a strain precision of ±1% required a subimage spacing of only 10 pixels (0.77 μm at a 2,500 magnification).

Figure 7 displays rendered strain maps for single black spruce latewood fiber. Accompanying displacement surfaces are displayed in Fig. 6. The fiber contained a number of microcompressive kinks or creases resulting from a modified preparation technique whereby two fibers were dried, one bridging the other. Strain components ϵ_{xx} and ϵ_{yy} indicated that a creased fiber cell wall results in large strain variations. A rational explanation of strain nonuniformity is offered.

Fiber strain distributions

The ESEM-based DIC system was successfully used for calculating the strain distributions of six defect-free black spruce latewood fibers under small applied strains of 0.3% to 0.5%. Component ϵ_{yy} indicated that straining in the direction of loading is distinctly nonuniform. Banded regions of high strain concentrations (0.9% to 8.8%), similar in character to Luders' bands which form in some metals (Illston et al. 1987), developed in the fiber wall under uniaxial tensile displacements. ϵ_{xx} was more uniform although strain concentrations of a lesser magnitude were evident. ϵ_{xx} was also largely negative, providing confirmatory evidence of a Poisson effect. These patterns were common to all defect-free fibers of black spruce latewood with a low microfibril angle tested in this preliminary study, the results of which are discussed in more detail in other sources (Mott 1995; Mott et al. 1995; Groom et al. 1995).

A reasonable explanation for strain nonuniformity was thought to be the manifestation of microcompressive defect "pull-out."

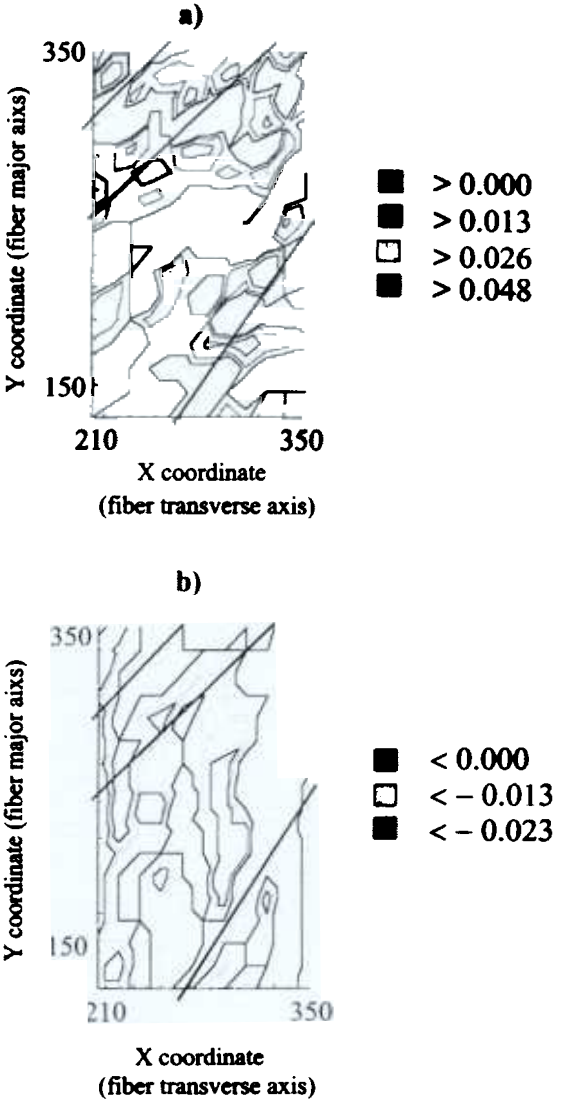

FIG. 7. Quantitative characterization of a) ϵ_{yy} and b) ϵ_{xx} in a micro-creased region of a wood fiber cell wall. The diagonal lines represent the approximate locations of the cell-wall defect creases. Applied strain = 0.53%. Initial subimage spacing = 13 pixels. Strain tolerance = 0.7%. A distinct Poisson effect was noticeable in all single fiber strain maps.

Microcompressive pull-out occurs as small crimps, creases, and kinks are removed from the cell wall under increasing tensile strain. Evidence of the high strain potential in microcompressively damaged regions is also

found when examining a fiber load elongation curve, which is frequently irregular and shallow in initial stages as the integrated effects of microcompressive pull-out take effect (Page and Seth 1980). A further potential cause of the strain band effect in the yy axis that cannot be discounted is the periodic and natural occurrence of amorphous cellulose regions and the presence of interstitial lignin or hemicellulose polymer phases of the cell-wall composite structure.

An initial assumption of DIC theory is that strain within any chosen subregion is uniform (Chu et al. 1985). This assumption was deemed valid when testing defect-free and minimally defected fibers. However, highly localized plastic deformations, such as those which occur around the tip of a growing crack in ductile materials, are problematic and would be difficult to measure unless small enough subregion areas were attainable. ESEM video microextensometry indicated that single fibers frequently display what can be considered a ductile cracking mechanism, characterized by a blunt crack tip. These cracks are commonly seen to extend from pit apertures and pit borders under increasing tensile displacement. Strain map pairs were rendered for several fibers that included a visible bordered pit. High strain concentrations were found to correspond with common displacement or load-induced crack locations at the pit aperture and at the pit border where the greatest S_2 layer microfibrillar deviation is known to occur.

The strain values close to the pit aperture were extremely large, however, and although representative of regions where high strain concentrations are likely to occur (they correspond to actual crack locations), the values are likely in error. The probable source of this error is a violation of the DIC assumption that strains within subregions be uniform (Chu et al. 1985). The failure of DIC to predict strain values in the locality of pits supported the hypothesis that large strain gradients exist in small regions ($< 1\ \mu m^2$) immediately adjacent to the aperture edge and that highly localized plastic deformation of this region was probable. A confirmed premature yielding of this type would have serious implications with regard to damage accumulation in single fibers subject to low repetitive or cyclic loading. The probable and potentially catastrophic premature plastic deformation of the cell wall in this study occurred in single fibers that were subject to applied strains of 1% or less.

CONCLUSIONS

ESEM-based DIC was used to determine single fiber microstrain distributions. Using present ESEM and DIC capabilities and carefully controlled fiber preparation techniques, it has been possible for the first time to measure single wood fiber Poisson effects, to quantify natural and induced cell-wall defects in terms of strain potential, and to explore and quantify single fiber failure mechanisms. Expected strain nonuniformity has been measured, and evidence for a quasi-ductile fracture mechanism and of a premature plastic failure region in the locality of natural defects now exists. For such analyses, a ± 0.1 pixel displacement measurement error and an optimum DIC subimage area of 29^2 pixels was adequate.

Smaller DIC measurement error, in the order of 0.01 pixel, now appears feasible using improved DIC algorithms (Lif et al. 1995). Improved computing facilities used in combination with such algorithms will promote faster DIC analyses and more precise data to confirm the initial findings of this study. For the present, however, ESEM-based DIC provides a powerful new tool to investigate the micromechanical process of fiber deformation and fracture, which together provide the bridge between fiber composite structure and morphology and mechanical properties. Investigation of this process is fundamental to the improvement of biocomposite materials.

ACKNOWLEDGMENTS

The authors would like to acknowledge the support of USDA NRI grant 94-37500-1199 and McIntire Stennis grant ME09607. In ad-

dition, the authors would like to thank Annukka Liukkonen and The University of Maine Paper Surface Science Program and Christopher Paduan for technical support. This is MAFES document No. 2004.

REFERENCES

CAMERON, R. E., AND A. M. DONALD. 1994. Minimizing sample evaporation in the environmental scanning electron microscope. J. Microscopy 173(3):227–237.

CHU, T. C., W. F. RANSON, M. A. SUTTON, AND W. H. PETERS. 1985. Applications of digital image correlation, techniques to experimental mechanics. Exp. Mech. Sept. 1995:232–244.

FUNG, Y. C. 1965. Foundation of solid mechanics. Prentice-Hall, Englewood Cliffs, NJ. P. 525.

GROOM, L. H., S. M. SHALER, AND L. MOTT. 1995. Characterizing micro- and macromechanical properties of single wood fibers. Pages 13–22 *in* Proc. 1995 International Paper Physics Conference. Sept. 11–14, Ontario, Canada.

ILLSTON, J. M., J. M. DINWOODIE, AND A. A. SMITH. 1987. Concrete, timber, and metals. The nature and behavior of structural materials. Van Nostrand Reinhold, London, UK. P. 378.

JAMES, M. R., W. L. MORRIS, B. N. COX, AND M. S. DADKHAH. 1989. Description and application of displacement measurements based on digital image processing. Micromechanics: Experimental Techniques. ASMR-AMD 102:89–99.

KORAN, Z. 1974. Intertracheid pitting in the radial cell walls of black spruce tracheids. Wood Sci. 7(2):111–115.

LIF, J. O., C. FELLERS, C. SOREMARK, AND M. SJODAHL. 1995. Characterizing the in-plane hygroexpansivity of paper by electronic speckle photography. J. Pulp Paper Sci. 21(9):302–309.

MOTT, L. 1995. Micromechanical properties and fracture mechanisms of single wood pulp fibers. Ph.D. dissertation, University of Maine Dept. of Forest Management, Orono, ME. P. 198.

———, S. M. SHALER, L. H. GROOM, AND B. H. LIANG. 1995. The tensile testing of individual wood fibers using environmental scanning electron microscopy and video image analysis. Tappi 78(5):143–148.

PAGE, D. H., AND F. EL-HOSSEINY. 1976. The mechanical properties of single wood pulp fibres. Pt. 4: The influence of defects. Sven. Papperstid. 14:471–474.

———, AND R. S. SETH. 1980. The elastic modulus of paper. 3. The effects of dislocations, microcompressions, curl, crimps, and kinks. Tappi 63(10):99–102.

———, F. EL-HOSSEINY, K. WINKLER, AND A. P. LANCASTER. 1977. Elastic modulus of single wood pulp fibres. Tappi 60(4):114–117.

PRESS, W. H., B. P. FLANNERY, S. A. TEUKOLSKY, AND W. T. VETTERLING. 1990. Numerical recipes in C. The art of scientific computing. Cambridge University Press, Cambridge, UK. P. 735.

SHEEHAN, G. S., AND L. E. SCRIVEN. 1991. Assessment of environmental scanning electron microscopy for coating research. Pages 377–383 *in* Proc. Tappi 1991 Coating Conference.

SIAU, J. F. 1984. Transport processes in wood. Springer Verlag, Berlin, Germany. P. 245.

WU, E. M., AND R. L. THOMAS. 1968. Off-axis test of a composite. J. Composite Mater. 2(4):523–526.

WUU, F., R. E. MARK, AND R. W. PERKINS. 1991. Mechanical properties of cut-out fibers in recycling. Pages 663–680, vol. 2 *in* Proc. International Paper Physics Conf. TAPPI Press, Atlanta, GA.

WOOD AND FIBER SCIENCE

(ISSN 0735-6161)

Volume 28 • October 1996 • Number 4

JOURNAL OF THE

SOCIETY OF WOOD SCIENCE AND TECHNOLOGY

SWST

(ISSN 0735-6161)
CODEN WOOFAJ

WOOD AND FIBER SCIENCE

JOURNAL OF THE SOCIETY OF WOOD SCIENCE AND TECHNOLOGY

VOLUME 28 OCTOBER 1996 NUMBER 4

CONTENTS

Editorial

WINISTORFER, PAUL M. The changing face of research ____ 389

Articles

LINDSTRÖM, HÅKAN. Basic density in Norway spruce. Part III. Development from the pith outwards ____ 391

PERALTA, PERRY N. Moisture sorption hysteresis and the independent-domain theory: The moisture distribution function ____ 406

NA, JAE SIK, DIDIER RONZE, AND ANDRÉ ZOULALIAN. Characterization of hydrolytic degradation of U-F joints through apparent diffusivity ____ 411

GARDNER, DOUGLAS J. Application of the Lifshitz-van der Waals acid-base approach to determine wood surface tension components ____ 422

MOTT, LAURENCE, STEPHEN M. SHALER, AND LESLIE H. GROOM. A technique to measure strain distributions in single wood pulp fibers ____ 429

ROUGER, FRÉDÉRIC. Application of a modified statistical segmentation method to timber machine strength grading ____ 438

VLOSKY, RICHARD P. Profile of furniture manufacturers in the U.S. South: Structure and industry growth factors ____ 450

OZANNE, LUCIE K., AND PAUL M. SMITH. Consumer segments for environmentally marketed wooden household furniture ____ 461

Books

SELLERS, TERRY, JR. Gluing wood, by Alberto Bandel ____ 478

SWST Distinguished Service Award ____ 479

George Marra Award ____ 480

Errata ____ 481

Guidelines and Procedures for George Marra Award ____ 482

SWST Accreditation ____ 483

Index ____ 484